Biogeosciences Discuss., 12, 4139–4181, 2015
www.biogeosciences-discuss.net/12/4139/2015/
doi:10.5194/bgd-12-4139-2015


Biogeosciences Discussions
Open Access



# On the vertical distribution of the chlorophyll *a* concentration in the Mediterranean Sea: a basin scale and seasonal approach

**H. Lavigne[1], F. D'Ortenzio[2,3], M. Ribera D'Alcalà[4], H. Claustre[2,3], R. Sauzède[2,3], and M. Gacic[1]**

[1]Istituto Nazionale di Oceanografia e di Geofisica Sperimentale – OGS, Dip. di Oceanografia, Borgo Grotta Gigante 42/c, 34010 Sgonico (Trieste), Italy
[2]CNRS, UMR 7093, Laboratoire d'Océanographie de Villefranche, 06230 Villefranche sur-Mer, France
[3]Université Pierre et Marie Curie-Paris 6, UMR 7093, Laboratoire d'Océanographie de Villefranche, 06230 Villefranche-sur-Mer, France
[4]Laboratorio di Oceanografia Biologica, Stazione Zoologica "A. Dohrn", Villa Comunale, Napoli, Italy







Received: 16 January 2015 – Accepted: 12 February 2015 – Published: 6 March 2015

Correspondence to: H. Lavigne (hlavigne@ogs.trieste.it)

Published by Copernicus Publications on behalf of the European Geosciences Union.





BGD
12, 4139–4181, 2015



## Abstract

The distribution of the chlorophyll *a* concentration ([Chl *a*]) in the Mediterranean Sea, which is mainly obtained from satellite surface observations or from scattered in situ experiments, is updated by analyzing a database of fluorescence profiles calibrated into [Chl *a*]. The database, which includes 6790 fluorescence profiles from various origins, was processed with a dedicated quality control procedure. To ensure homogeneity between the different data sources, 65 % of fluorescence profiles have been inter-calibrated on the basis of their concomitant satellite [Chl *a*] estimation. The climatological pattern of [Chl *a*] vertical profile in four key sites of the Mediterranean Sea has been analyzed. Climatological results confirm previous findings on the range of [Chl *a*] values and on the main Mediterranean trophic regimes. It also provides new insights on the seasonal variability of the shape of the vertical [Chl *a*] profile, inaccessible from remote sensing observations. An analysis based on the recognition of the general shape of the fluorescence profile was also performed. Although the shape of [Chl *a*] vertical distribution characterized by a deep chlorophyll maximum (DCM) is ubiquitous during summer, different forms are observed during winter, suggesting thus that factors affecting the vertical distribution of the biomass are complex and highly variable. The [Chl *a*] distribution in the Mediterranean Sea mimics, at smaller scales, what is observed in the Global Ocean. As already evidenced by analyzing satellite surface observations, mid-latitude and subtropical like phytoplankton dynamics coexist in the Mediterranean Sea. Moreover, the Mediterranean DCM variability appears characterized by patterns already observed at global scale.





BGD
12, 4139–4181, 2015



## 1 Introduction

### 1.1 Surface chlorophyll distribution

Chlorophyll *a* concentration ([Chl *a*] hereafter) is the main proxy of phytoplankton biomass (Strickland, 1965; Cullen, 1982) and represents a key oceanic biogeochemical variable. However, in the Mediterranean Sea, as in the global ocean, the lack of in situ observations (Conkright et al., 2002; Manca et al., 2004) has prevented a comprehensive knowledge of the [Chl *a*] spatio-temporal variability. The understanding of the [Chl *a*] distribution is essentially restrained to surface, as based on remote sensing observations. In the Mediterranean Sea, the ocean color sensors, like CZCS (Feldman et al., 1989) or SeaWiFS (McClain et al., 1998), provide observations with high temporal and spatial resolution over the whole basin (Morel and André, 1991; Antoine et al., 1995; Bosc et al., 2004).

As shown from in situ observations (Dolan et al., 1999, 2002; Ignatiades et al., 2009), satellite data confirmed the ultra-oligotrophic nature of the basin (Dugdale and Wilkerson, 1988) and the east–west gradient in the oligotrophy. Except for the Liguro-Provençal region, where a large spring bloom takes place, and for some localized spots, most of the basin exhibits very low values ($< 0.2\,mg\,m^{-2}$) of satellite surface [Chl *a*]. Surface [Chl *a*] decreases eastward (Bosc et al., 2004; Barale et al., 2008) and displays a sharp gradient between the west and east basins (mean [Chl *a*] is about $0.4\,mg\,m^{-3}$ in the west basin and $0.05\,mg\,m^{-3}$ in the east basin, Bosc et al., 2004). Superimposed on this general pattern, ocean color data provided also insights on the occurrence and on the influence of meso and sub-mesoscale structures on [Chl *a*] (Taupier-Letage et al., 2003; Navarro et al., 2011; D'Ortenzio et al., 2014).

Satellite observations were also the primary source of information for the characterization of the [Chl *a*] seasonal and interannual variability (D'Ortenzio and Ribera d'Alcalà, 2009; Volpe et al., 2012; Lavigne et al., 2013). At global scale, ocean color satellite observations indicate that surface [Chl *a*] annual cycles switch from a tropical to a temperate or a polar environment (Yoder et al., 1993) following generally latitu-





BGD
12, 4139–4181, 2015



dinal gradients. Boundaries between large ecological regions have been determined from satellite observations, in the global ocean (Longhurst, 2006) but also at regional scales (Devred et al., 2007; D'Ortenzio and Ribera d'Alcalà, 2009; Platt et al., 2010). Indeed, in the Mediterranean, a satellite based bioregional approach confirmed previous observations (D'Ortenzio and Ribera d'Alcalà, 2009); authors demonstrated that a subtropical-like [Chl *a*] seasonality (highest [Chl *a*] during winter and lowest during summer) encompasses most of the basin whereas a temperate like seasonality, marked by a high peak of surface [Chl *a*] in spring (in March/April), is recurrently observed in the North-Western basin and occasionally in other Mediterranean regions. Further analysis (Lavigne et al., 2013) showed that the coexistence of different regimes in the Mediterranean Sea is mainly due to the high variability of the interplay between physical forcing, which affects the mixed layer depth (MLD hereafter), and chemical forcing (i.e. nutrients availability).

### 1.2 The vertical [Chl *a*] distribution

The vertical distribution of [Chl *a*] is mainly determined by external forcing like the penetration of light in water, the MLD or the nutrient distribution (Estrada et al., 1993; Ward and Waniec, 2007). From space, however, only a small part of the vertically integrated [Chl *a*] content is detected and the [Chl *a*] vertical distribution is missed. In the Mediterranean Sea, which is characterized by a strong oligotrophy and by the ubiquitous occurrence of a deep chlorophyll maximum (DCM, hereafter), this limitation inherent to satellite observation is particularly critical.

DCMs have been observed everywhere over the Mediterranean from spring to autumn (Crise et al., 1999; Moutin and Raimbault, 2002; Siokou-Frangou et al., 2010). A longitudinal deepening of the DCM has been also documented (see Crise et al., 1999 for a review). DCM depths range from 30 m in the western most area (Dolan et al., 2002) to 70 m in the South Adriatic and to more than 100 m in the Levantine Sea (Christaki et al., 2001). Mediterranean DCMs are also impacted by 3-D processes such as lateral advection, upwelling and eddy transport (Crise et al., 1999; Estrada et al., 1993).





BGD
12, 4139–4181, 2015



Previous studies indicated that Mediterranean DCM coincides with biomass maximum (Mignot et al., 2014; Macias et al., 2014) and thus significantly contributes to vertically integrated primary production (Estrada et al., 1993; Macias et al., 2014). However, because of the impact of photo-adaptation processes (Cullen, 1982; Winn et al., 1995), the amplitude of the DCM is much larger, and not representative, of the amplitude of the subsurface biomass peak (Mignot et al., 2014).

Overall, little is known about other shapes (i.e. without DCM) of the [Chl *a*] vertical distribution. Most of the existing observations are obtained for locations where regular sampling provided a seasonal and/or interannual picture of the variability of [Chl *a*] (e.g. DYFAMED station, Marty et al., 2002; Cretan Sea, Psarra et al., 2000; Levantine Sea, Krom et al., 1992). DCMs are not observed in the Mediterranean during strong winter mixing episodes (Siokou-Frangou et al., 2010), or, more generally, during winter. During this season, a so called "mixed" shape (Morel and Berthon, 1989; Uitz et al., 2006), characterized by a constant [Chl *a*] from the surface to the basis of the MLD, is often observed, in both western and eastern basins (Krom et al., 1992; Marty et al., 2002; Mignot et al., 2014). Alternatively, a [Chl *a*] vertical shape marked by a high subsurface maximum close to the surface (less than 10 m) have also been documented for the North-Western basin, during the spring bloom period (Marty et al., 2002; Manca et al., 2004).

The lack of knowledge on the vertical [Chl *a*] distribution is mainly due to the costly and difficult in situ [Chl *a*] measurements. Standard method requires seawater samples, which are further filtered to concentrate biomass. The filters are then analyzed in laboratory with fluorometric, spectrophotometric or chromatographic methods. A good accuracy in the estimation of [Chl *a*] is then obtained, especially when High Performance Liquid Chromatography (HPLC, Gieskes and Kraay, 1983) is used. The associated protocols are, however, expensive, time consuming and it only provides discrete estimations. Consequently, compared to other physical (e.g. temperature and salinity) and even biogeochemical (e.g. oxygen) parameters, [Chl *a*] Mediterranean data are very scarce (Manca et al., 2004). However, attempts to group in situ [Chl *a*] observations to





BGD
12, 4139–4181, 2015



characterize seasonal and spatial [Chl *a*] variability at Mediterranean scale have been realized, resulting in the production of a [Chl *a*] climatology (the MEDAR/MEDATLAS project, Maillard et al., 2005). As expected, however, the vertical resolution of the climatological [Chl *a*] field is weak (12 points on the vertical) and only seasonal estimations are available.

### 1.3 Fluorescence

A way to overcome the scarcity of water sample derived [Chl *a*] data, is to use fluorescence observations to increase the number of available profiles. The estimation of [Chl *a*] from the fluorescence technique (Lorenzen, 1966) is based on the chlorophyll *a* property of absorbing blue light and re-emitting it, as fluorescence, in the red part of the spectrum. The quantity of fluorescence emitted by water sample is proportional to [Chl *a*], which could be then easily derived by measuring emitted radiation at red wavelengths. The fluorescence technique represents then a robust and non-invasive method to observe continuous vertical profiles of [Chl *a*]. Because of the simplicity of the in situ fluorescence measurements and the increasing number of profiling floats and gliders equipped with a fluorometer (Johnson et al., 2009), the fluorescence is becoming the main source of data for [Chl *a*] vertical profiles (more than 67 900 fluorescence profiles in the World Ocean Database, 2013; Boyer et al., 2013).

Fluorescence, however, is only a proxy for [Chl *a*], in the sense that a calibration of the fluorescence signal is required to obtain [Chl *a*] estimation. Generally, calibration coefficients ($\alpha$ and $\beta$, see Eq. 1) as provided by manufacturers, do not generally reach the accuracy required for scientific applications. The main issue with fluorescence is the high variability of the fluorescence to [Chl *a*] ratio since it changes with the taxonomic assemblage or the environmental conditions (Kiefer, 1973). For instance, under low light conditions, the chlorophyll content per cell can increase and the fluorescence to [Chl *a*] ratio decreases due to the packaging effect (Sosik et al., 1989). In response to supra-optimal light irradiation, phytoplankton triggers photo-protection mechanisms, inducing a drastic decrease of the fluorescence to [Chl *a*] ratio (Kolber and Falkowski,





BGD
12, 4139–4181, 2015



1993; Müller et al., 2001); this mechanism is named Non Photochemical Quenching (NPQ). The main result of NPQ effect is a decrease of fluorescence at the surface, not paralleled by a diminution of the [Chl *a*] (Cullen and Lewis, 1995; Xing et al., 2012).

$$[\text{Chl } a] = \alpha \cdot (\text{FLUO} - \beta) \quad (1)$$

Improved protocols are based on the determination of calibration coefficients (i.e. $\alpha$ and $\beta$) by comparing fluorescence with in situ data, for each profile (Morel and Maritorena, 2001) or for each cruise (Sharples et al., 2001; Strass, 1990; Cetinic et al., 2009). However, this calibration method based on simultaneous in situ samples is not always applicable. Alternative calibration methods, not dependent on concomitant HPLC observations, have been then recently developed (Boss et al., 2008; Xing et al., 2011; Mignot et al., 2011; Lavigne et al., 2012). Using additional information like the irradiance profiles (Xing et al., 2011), the simultaneous availability of ocean color observations (Boss et al., 2008; Lavigne et al., 2012) or the only knowledge of the shape of the chlorophyll fluorescence profile (Mignot et al., 2011) calibration methods were proposed, tested and validated. Although these new calibration methods do not attain the accuracy of the HPLC based calibration, they offer an acceptable alternative to calibrate a large quantity of fluorescence profiles in a unique way.

### 1.4 Outlines

This study aims to improve our knowledge of the spatio-temporal variability of the vertical distribution of the [Chl *a*] in the Mediterranean Sea, focusing especially on [Chl *a*] seasonality. In this basin, ocean color observations showed that surface chlorophyll seasonal cycle is characterized by a mid-latitude or a sub-tropical pattern (D'Ortenzio and Ribera d'Alcalà, 2009; Lavigne et al., 2013), although little is known about the [Chl *a*] seasonality in subsurface and deep layers. The shape of the vertical distribution of [Chl *a*] is also carefully analyzed here, as different forms could be indicative of different processes controlling the distribution of phytoplankton. The variability of the





BGD
12, 4139–4181, 2015



DCM, which is one of the most ubiquitous feature of the Mediterranean [Chl *a*] vertical shapes, will be also specifically investigated.

In the next section, the fluorescence database used is presented as well as the quality control and the calibration procedures that were applied. In the result section, the seasonal and spatial variability of climatological [Chl *a*] vertical profiles, derived from fluorescence-based reconstructed [Chl *a*] profiles is presented. Climatological results are completed by the analysis of the shape of the [Chl *a*] profiles. The seasonal variability of occurrences of the main observed shapes for [Chl *a*] vertical profiles is investigated here. In the Sect. 4, some methodological points related to the production of climatological patterns are addressed. Results presented in the previous section are also discussed against previous remote sensing based observations and finally, Mediterranean diversity in [Chl *a*] patterns is highlighted with a comparison to the Global Ocean.

## 2 Data and methods

### 2.1 Data set of fluorescence chlorophyll profiles

More than 6000 chlorophyll fluorescence profiles, and their corresponding temperature and salinity profiles, obtained in the Mediterranean Sea (regions where bathymetry exceeds 100 m depth) were collected from various data sources (Table 1) which comprise online databases (986 profiles), some French cruises (2670 profiles), the MEDAR (228 profiles) and the SESAME programs (1815 profiles) and finally fluorescence profiles derived from Bio-Argo floats (1091 profiles). Profiles density covers the whole Mediterranean Basin, although some areas are better represented than others (Fig. 1). Many profiles are available in the North-Western Mediterranean Sea, whereas the South-Western Mediterranean Sea and the Levantine Sea are poorly represented. Available profiles spread over the 1994–2014 period and all seasons are equally represented (winter 30 % of data, spring 21 %, summer 25 % and autumn 24 %).





BGD
12, 4139–4181, 2015



## 2.2 Data processing and calibration

Before calibration, a quality control procedure was applied to fluorescence profiles. It comprises a test of uniqueness, the identification of the spikes (see D'Ortenzio et al., 2010) and of the signs of fluorometer failure (portion of profile with exactly the same value or jumps in the fluorescence profile). After the application of quality control, 593 profiles were removed from the database. Then, too shallow profiles (i.e. profiles for which the acquisition was not deep enough to display the whole fluorescence shape) were also removed. Practically, profiles with a surface fluorescence value lower than the bottom value were removed from the database (202 profiles removed). In addition, profiles achieved in the Ionian Sea during the "Long Duration" station B of the BOUM cruise (Moutin et al., 2012) were removed from our dataset as sampled at very high temporal frequency an anticyclonic eddy (Moutin and Prieur, 2012). These 121 profiles, which are not independent, over-represent in the dataset a specific structure of the Ionian Sea.

The remaining fluorescence profiles (5854 profiles) were calibrated using satellite ocean color matchups as surface reference (Lavigne et al., 2012). This method has been validated in the Mediterranean Sea, by comparing satellite calibrated profiles and in situ HPLC [Chl *a*] data. In the Mediterranean Sea, the calibrated profiles are unbiased and present a median error of 41 %, which is reduced to 34 % when climatological averages are compared. To summarize, (see Lavigne et al., 2012, to a comprehensive description and validation of the procedure) the method consists in (step 1) a correction for the NPQ effect, (step 2) an adjustment to a zero value of the fluorescence profile at depth and (step 3) an application of a calibration coefficient obtained from ocean color satellite matchups. The last step has been applied only to the fluorescence profiles available for the period 1998–2014 (i.e. period during which the SeaWiFS or MODIS Aqua data are available and can be used to calculate the matchups).

The step 1 provides a systematic correction of the NPQ effect by extrapolating up to the surface the maximum fluorescence value observed in the mixed layer (Xing





BGD
12, 4139–4181, 2015



et al., 2012). The MLD was evaluated from potential density profiles using a density criterion of 0.03 kg m$^{-3}$ (de Boyer Montegut et al., 2004; D'Ortenzio et al., 2005). This method revealed to be efficient to correct NPQ (Xing et al., 2012; Lavigne et al., 2012) although it has limits when MLD is shallow and water column is stratified.

Step 2 corrects systematic instrumental offset, which impacts on the whole profile, although it could only be detected at depth. Except for very specific cases, [Chl *a*] is supposed to be zero where depth is deep enough to prevent light availability. If it is not the case, a correction factor (i.e. $\beta$ on Eq. 1) is subtracted to the whole fluorescence profile to impose that the median of the ten deepest observations is equal to zero. Profiles in which MLD was deepest than the deepest fluorescence observation were not treated (1.1 % of data set). After step 1 and step 2 procedures, 5854 profiles were successfully corrected and stored in the so-called "1994–2014 database". These fluorescence profiles were used for the shape analysis see Sects. 2.3 and 3.2.

In step 3, fluorescence profiles achieved after 1998 were converted into [Chl *a*] units using a transformation based on the ocean color satellite observations (Lavigne et al., 2012). The 8 day Level 3 standard mapped images of SeaWiFS and MODIS Aqua surface chlorophyll at 9 km resolution were obtained from the NASA web site (http://oceancolor.gsfc.nasa.gov/) for the 1998–2014 period (1998–2007 for SeaWiFS and 2008–2014 for MODIS Aqua). The use of NASA [Chl *a*] standard products allows for a good consistency between SeaWiFS and MODIS datasets and avoids the introduction of any bias between the two time-series (Franz et al., 2005). For each fluorescence profile, the satellite image matching the date of profile was selected. The corresponding surface [Chl *a*] values over a $0.1^\circ \times 0.1^\circ$ box centered on the geographical position of the profile were extracted and averaged. The integrated chlorophyll content over $1.5Z_e$ (where $Z_e$ is the euphotic depth) is then estimated from satellite [Chl *a*] using empirical relationships (Uitz et al., 2006). A multiplicative coefficient ($\alpha$ coefficient in Eq. 1) is applied to the fluorescence profile, imposing that the integrated fluorescence content matches the value derived from satellite. At the end, 4150 fluorescence profiles were successfully transformed into [Chl *a*]. These [Chl *a*] profiles formed the "1998–





BGD
12, 4139–4181, 2015



2014 database" and similarly to fluorescence profiles of the "1994–2014 database", they are available upon request from the first author.

### 2.3 Determination of the shape of fluorescence profiles

On the basis of a visual analysis of the whole database, five general types of fluorescence vertical shape were identified. The five categories, which represent the most frequent shapes of vertical distribution observed in the Mediterranean, also reflect the physical-biological processes determining them. These categories are referred as "DCM", "homogeneous", "HSC" (for high surface chlorophyll), "complex" and "modified DCM" on the basis of their general characteristics (Fig. 2). The "DCM" and "homogeneous" shapes are commonly used to describe chlorophyll vertical profiles (Morel and Berthon, 1989; Uitz et al., 2006; Mignot et al., 2011). The "DCM" shape corresponds to the typical "stratified shape" (Cullen, 1982), characterized by a subsurface DCM, while the "homogeneous" shape, corresponds to the already identified "mixed shape" (Morel and Berthon, 1989; Uitz et al., 2006), characterized by a positive homogeneous [Chl *a*] in the mixed layer. Examining the database, three other standard shapes have been introduced (i.e. "HSC", "modified DCM" and "complex" shapes) to better describe the variability observed. The "HSC" standard shape was defined for profiles displaying a steady decrease of [Chl *a*] from surface to depth ($\sim$ 100 m) as previously observed during phytoplankton bloom (Chiswell, 2011). The "modified DCM" shape describes profiles with relatively high values in the mixed layer and with a peak of [Chl *a*] just below the MLD. It represents an intermediate condition between the "DCM" and "homogeneous" situations. Finally, profiles with a complex shape, often displaying several peaks and a relatively high [Chl *a*] in surface were referred to the "complex" standard shape.

To automatically categorize the profiles of the 1994–2014 database in one of the five standard shapes, a simple algorithm has been used, computing for each profile the following metrics: the depth of fluorescence maxima ($D_{max}$, see Fig. 2a and f), the MLD, the fluorescence integrated content in a 20 m layer centered on $D_{max}$ ($F_{max}$, see





BGD
12, 4139–4181, 2015



Fig. 2a), the fluorescence integrated content in the 0–20 m surface layer ($F_{surf}$, see Fig. 2a), the fluorescence integrated content in the mixed layer ($F_{MLD}$, see Fig. 2f) and the total fluorescence content ($F_T$, see Fig. 2b).

The algorithm was applied to each profile. First, it tests for the "DCM" shape. If MLD is above $D_{max}$ and if $F_{max}$ is twice superior to $F_{surf}$, the profile is classed in the "DCM" category. If not, the "homogeneous" shape is tested. The profile is classed in the "homogeneous" category if $F_{MLD}/F_T$ is superior to 0.85 (more than 85 % of biomass is contained in the mixed layer). Then, the "HSC" shape is tested. The "HSC" shape is assigned to a profile if its fluorescence averaged over layers of 10 m width decreases from surface to 100 m. Finally, if the fluorescence profile does not meet any of the previous criteria, it is classed in the "modified DCM" category if its MLD is above $D_{max}$ or in the "complex" category otherwise.

Overall, 3063 profiles were classed in the "DCM" category, 751 in the "homogeneous" category, 413 in the "HSC" category, 637 in the "modified DCM" category and 990 in the "complex" category.

## 3 Results

### 3.1 Some climatological behaviors

Although the availability of the calibrated profiles (1998–2014 database) should allow generating interpolated products on regular mesh grid (as for example the World Ocean Atlas, Conkright et al., 2002), we preferred to avoid any hard interpolation and only present Mediterranean patterns for locations well represented in our database. Hence, monthly climatologies of [Chl *a*] vertical profiles were computed for four geographical points around which the data density was high. These points were also placed in four main Mediterranean sub-basins (i.e. 42° N/5° E in the North Western basin, 38° N/5° E in the South-Western basin, 36° N/17° E in the Ionian Sea and 33.5° N/33° E in the Levantine Sea, see yellow diamonds on Fig. 1). The monthly climatological time-series are





BGD
12, 4139–4181, 2015



presented in the next section (Sect. 3.1.1). Then, to better identify spatial changes in [Chl *a*] fields, we also present climatological transects (Sect. 3.1.2). The weak density of data in the eastern basin, only allows us to analyze [Chl *a*] distribution along a 5° E north–south transect in the western basin (see dotted line on Fig. 1). As this transect encompasses regions with different biological dynamics (D'Ortenzio and Ribera d'Alcalà, 2009), it represents a great interest.

### 3.1.1 Seasonality in four geographic points

For each of the four selected geographic points (see above), all available profiles in a $4^\circ \times 4^\circ$ side box centered on the chosen geographical position were averaged on a 1 m vertical scale and on a monthly basis to produce climatological profiles. The resulting monthly climatologies are displayed on Fig. 3.

Overall, the climatological time-series representing the South-Western basin, the Ionian Sea and the Levantine Sea (Fig. 3b–d) display a similar evolution of the vertical [Chl *a*] distribution. From December to March, [Chl *a*] is greater in the surface layers (Fig. 2b), while the April to November months are characterized by the occurrence of a DCM. In the South-Western region, winter profiles present relatively high [Chl *a*] in the upper 70 m ([Chl *a*] $> 0.5\,\mathrm{mg\,m^{-3}}$), whereas in the Ionian, and even more in the Levantine, upper layer [Chl *a*] is lower and the depth of the layer in which [Chl *a*] is not zero is deeper (about 150 m in the Ionian Sea and more than 200 m in the Levantine Sea). DCM, when occurring, is deeper in the Levantine and Ionian seas than in the South-Western region. The climatological time-series in the North-Western basin (Fig. 3a) displays a different succession. The presence of [Chl *a*] accumulation in surface and subsurface layers (Fig. 2c) is observed in March and April, and, in a minor extent from November to February. DCM occurs from May to October. Finally, all time-series are characterized by a deepening of the DCM from May to July and a shallowing from August to September.

Regarding [Chl *a*] values, regional differences are visible and confirm previous observations about the increase of the oligotrophy from west to east. The highest [Chl *a*]





BGD
12, 4139–4181, 2015



value is observed in April, in the North-Western climatology (Fig. 3a) and it reaches 1.2 mg m$^{-3}$. Note however, that this mean value is derived from extremely variable observations in the range between 0.3 and 4.2 mg m$^{-3}$. The South-Western time-series shows [Chl *a*] values up to 0.5 mg m$^{-3}$, observed in the surface during winter and at DCM during summer. In the Ionian climatology, highest [Chl *a*] values can be observed at DCM, they reach 0.3 mg m$^{-3}$. Finally, the Levantine climatology displays the lowest [Chl *a*], with values rarely exceeding 0.25 mg m$^{-3}$.

Table 2 indicates on the averaged [Chl *a*] values at DCM depth for each of the four geographic points analyzed here. Contrary to the DCM [Chl *a*] values visible on Fig. 3, the values reported on Table 2 derived from the averaging of the DCM [Chl *a*] values extracted individually on each fluorescence profile presenting a DCM. In the North-Western region, [Chl *a*] at DCM is often around 1 mg m$^{-3}$ but ranges between 0.65 mg m$^{-3}$ in September and 1.22 mg m$^{-3}$ in April. At the South-Western point, the averaged [Chl *a*] at DCM is 0.87 mg m$^{-3}$. In the Eastern basin, values are twice lower (about 0.55 mg m$^{-3}$ at the Ionian point and 0.45 mg m$^{-3}$ at the Levantine point). A seasonal pattern does not clearly emerge from the analysis of the DCM statistics, except that [Chl *a*] at DCM is generally higher during spring and summer and lower during autumn. Note that averaged DCM depth [Chl *a*] values (Table 2) are highest than DCM depth [Chl *a*] values observed on climatological profiles (Fig. 3) because the averaging process on the latter tends to flat DCMs (see discussion on Sect. 4.1.2, Lavigne et al., 2012).

### 3.1.2 North–South transect

All the data located in a surface of ±2° from the 5° E meridian were selected to produce climatological pictures of [Chl *a*] field at spring (March–May, Fig. 4a) and summer (June–September, Fig. 4b).

The spring situation (Fig. 4a) displays various types of profiles and a large range of [Chl *a*] values. North of 41° N, [Chl *a*] values are high (> 1 mg m$^{-3}$) in surface and decrease with depth. Highest [Chl *a*] values (~ 3 mg m$^{-3}$) are observed around 42° N in





BGD
12, 4139–4181, 2015



surface (up to 30 m depth). Between 40 and 41° N, surface [Chl *a*] is around 0.5 mg m$^{-3}$ and a DCM is visible at 50 m depth. Southward, the climatological transect displays a deeper DCM (around 75 m depth) and very low surface [Chl *a*] values (< 0.3 mg m$^{-3}$).

In the summer transect (Fig. 4b), the presence of a DCM is ubiquitous, though its position in the water column and its [Chl *a*] values vary throughout the transect. A steady deepening of the DCM is observed from 43° N (DCM depth around 50 m) to 39° N (DCM depth around 85 m). A decrease of [Chl *a*] at DCM is also observed southward. It ranges from 0.8 to 0.4 mg m$^{-3}$. South of 39° N, a shallowing of the DCM depth and an increase of the [Chl *a*] at DCM are observed.

## 3.2 Analysis of the profile shapes

### 3.2.1 Seasonal distribution of the profile shapes

As a procedure was established to classify the shapes of the [Chl *a*] profiles included in the 1994–2014 database (Sect. 2.3), an objective study of their seasonal distributions in main Mediterranean regions is possible (Fig. 5). Boundaries of main Mediterranean regions are drawn in the Fig. 1.

During summer, all regions are dominated by the "DCM" shape with occurrences exceeding 90 %. DCM definitively disappears in November everywhere, although the start of its formation varies with regions: in April for the Ionian, Levantine and Tyrrhenian regions, in May for the South-West region and in June for the North-West region. During the autumn/winter period, all the shapes are observed in a same region and in a same month. Nevertheless, profiles with the "modified DCM" shape are more frequent in early winter (see for instance the Ionian region where the "modified DCM" shape represents more than 60 % of profiles in December and January). Profiles with the "homogeneous" shape are observed from November to March, except in the Ionian region. Similarly, the "complex" shape is presented everywhere from November to March. Profiles displaying a "HSC" shape are absent, or nearly absent, of the Ionian and Levantine regions. In the Tyrrhenian and South-West regions, "HSC" profiles can





BGD
12, 4139–4181, 2015



be observed between November and March and are the most abundant in February. In the North-West region, although "HSC" profiles are observed in winter, from November to February, they peak at spring (March–April) with occurrences exceeding 60 %.

### 3.2.2 Longitudinal and seasonal distribution of the DCM depth

DCM shape is confirmed to be a dominant feature of the [Chl *a*] distribution in the Mediterranean, although its characteristics change from a region to another and with time. A deepening of the DCM depth with the longitude is generally observed (Fig. 6), confirming previous findings (Crise et al., 1999). A linear model applied to DCM depth data indicates that, on average, DCM depth deepens by 1.6 m for 1° of longitude. However, a large variability exists, especially in the Ionian and Levantine seas. Superimposed to this general deepening of DCM with longitude, regional differences can be observed between the main Mediterranean sub-basins. Considering profiles at the same range of longitude, the averaged DCM depth is deeper and more variable in the South-West region (mean = 73 m, SD = 18.7 m) than in the North-West region (mean = 52 m, SD = 12.5 m). In the eastern basin, the Adriatic region displays shallow and stable DCM depths (mean = 56 m, SD = 10.1 m) whereas the Ionian and Levantine regions display deeper and more variable DCM depths (mean = 75 m, SD = 21.5 m for Ionian, mean = 102 m, SD = 16.9 m for Levantine).

The variability observed in the different Mediterranean regions can be partially explained by the seasonality. All Mediterranean regions have a seasonal variability in the DCM depth (Fig. 7) which is characterized by a widespread deepening from March to mid-summer and a shallowing from mid-summer to November. In all Mediterranean regions, except the North-West region, the spring to summer deepening of the DCM is of 40 % (in the North-West region it is of 33 %).





BGD
12, 4139–4181, 2015



## 4 Discussion

### 4.1 Discussion on method

#### 4.1.1 Comparison with MEDATLAS

The climatological profiles for each of the four geographical points analyzed in the Sect. 3.1 have been computed from the MEDATLAS climatology and compared with their fluorescence based counterparts (Fig. 8). For each geographical point, the two versions of [Chl *a*] vertical profiles (fluorescence based and MEDATLAS) display similar ranges of values, although differences are observed in the form of [Chl *a*] vertical profiles. The fluorescence based profiles often display thinner DCMs with higher [Chl *a*] values than in the MEDATLAS climatology (see for instance Fig. 8b summer, c autumn and d summer). Moreover, in the MEDATLAS climatology, very weak seasonal changes of the DCM depth are visible. These divergences can be explained by the use of discrete data and of interpolation in the MEDATLAS climatology, which prevents the proper characterization of vertical structures like DCMs. In winter, the MEDATLAS climatology, and sometimes the fluorescence based climatology, shows profiles with subsurface maxima (Fig. 8a–c, winter), which are not observed in the monthly fluorescence based time-series (Fig. 3). We hypothesize that these winter subsurface maxima could be an artifact caused by the large averaging period (from December to March), which drive to merge [Chl *a*] profiles with highly different vertical distributions (see Fig. 5).

#### 4.1.2 Methodological approaches

In the present study, two different approaches have been used to describe the monthly variability of [Chl *a*] profiles. On one hand, the "standard" method, consisting in averaging [Chl *a*] values for some defined standard depths (Conkright et al., 2002, Sect. 3.1). On the other hand, a "probabilistic" method (Sect. 3.2), where each [Chl *a*] profile was considered as a whole, focusing the analysis on its general shape and on specific fea-





BGD
12, 4139–4181, 2015



tures (e.g. DCM depth). The second approach requires the a priori knowledge of the main shapes of profile existing in the database and the definition of an efficient and automatic procedure to categorize the profiles. In this study, the main standard shapes and the classification procedure have been defined after the individual visualization of all the fluorescence profiles of the database as well as their characteristics (i.e. $D_{max}$, $F_{MLD}/F_T$, $F_{max}/F_{surf}$, see Sect. 2.3 for details).

The two approaches are complementary. The "standard" method highlights the average pattern of the [Chl *a*] profile and informs about the ranges of values for [Chl *a*]. However, [Chl *a*] values has to be considered independently for each depth and the shape of the resulting climatological profile has to be interpreted carefully because it is a composite. A typical artifact of this method is the tendency of the DCM to be flattened (compare DCM of Fig. 3 and values of Table 2). In these cases (i.e. [Chl *a*] profile extremely stable, as during summer, or very dynamic, as during winter), the "probabilistic" analysis of the shape of the [Chl *a*] profile appears more pertinent. It showed that seasonal changes in [Chl *a*] profiles are not smooth and steady, like the climatological analysis may suggest, but highly dynamic. This approach reveals then the complexity and variability of factors influencing the vertical distribution of biomass (i.e. vertical mixing, 3-D dynamic structures, light distribution, grazing pressure, Longhurst and Harrison, 1989, see also discussion below).

## 4.2 A new vision of the [Chl *a*] in the Mediterranean Sea

### 4.2.1 Comparison to previous satellite ocean color observations

The main feature that emerges from the analysis of annual cycles of surface [Chl *a*] from ocean color data over the Mediterranean sea is the coexistence of two main types of cycle (Bosc et al., 2004; D'Ortenzio and Ribera, 2009; Lavigne et al., 2013). The two cycles ("NO BLOOM" and "BLOOM", following the definition of D'Ortenzio and Ribera d'Alcalà, 2009) are characterized, the first, by an increase of normalized [Chl *a*] by a factor up to 2 from summer to winter (NO BLOOM annual cycle) and, the second, by





BGD
12, 4139–4181, 2015



a moderate increase of normalized [Chl *a*] (factor 2) from summer to winter, followed by an exponential increase (factor 3) in early spring (BLOOM annual cycle). Although these previous findings are based on satellite surface [Chl *a*] and result from a complex statistical analysis (i.e. normalization of the seasonal cycles, clustering analysis), they are confirmed by some of the climatological time-series presented here (see Sect. 3.1). Climatologies of [Chl *a*] profiles (Fig. 3) for the South-Western region (Fig. 3b), the Ionian region (Fig. 3c) and the Levantine region (Fig. 3d) which correspond to the NO BLOOM regions identified by D'Ortenzio and Ribera d'Alcalà (2009) not only display similarities in the seasonal variations of surface [Chl *a*] but they also showed the same succession of winter homogeneous profiles and summer profiles with DCM. In contrast, the time-series corresponding to the North-Western region (Fig. 3a) presents, in March and April, [Chl *a*] vertical profiles characterized by high surface concentrations (i.e. Bloom profiles) and confirm the special feature of the North-Western region in the Mediterranean Sea.

Beyond the bimodal conception (i.e. BLOOM/NO BLOOM) of annual biomass cycles in the Mediterranean Sea, there is an important and unresolved complexity marked by the presence of regional differences inside of the two main biomass annual cycles. One of the best illustration of this complexity is the identification by D'Ortenzio and Ribera d'Alcalà (2009) of three different annual cycles (i.e. 3 bioregions) for the NO BLOOM dynamic. The probabilistic analysis of the general shape of the [Chl *a*] profiles achieved in this paper also contributes to refine the basic BLOOM/NO BLOOM scheme and should help to explain the complex patterns observed from surface. In Fig. 5 regional differences in the distribution of the standard shapes for [Chl *a*] vertical profiles are observed among the NO BLOOM regions (i.e. South-West, Levantine and Ionian regions). The main difference is probably the significant proportion of "HSC" like profiles during winter months (i.e. January, February and March) in the South-West region whereas this proportion is very small (less than 10 %) in the Ionian sea and even zero in the Levantine Sea. The observation of "HSC" like profiles in the South-West region suggests that, during winter, mixing is able to supply enough nutrients in surface to al-





BGD
12, 4139–4181, 2015



low for episodic developments of phytoplankton close to the surface, like small blooms, when water column begin to stabilize. That could also explain the higher [Chl *a*] observed in the South-West region and the difference between the South-Western [Chl *a*] normalized annual cycle and the Eastern ones (D'Ortenzio and Ribera d'Alcalà, 2009).

#### 4.2.2 High diversity of the Mediterranean [Chl *a*]

Although Mediterranean Sea spreads over a relatively small latitudinal range (from 30 to 45° N), previous findings, essentially based on satellite observations, have shown that in this basin annual phytoplankton cycles representative of subtropical and mid-latitude regions of the global ocean coexist (D'Ortenzio and Ribera d'Alcalà 2009; Lavigne et al., 2013). Present results, which focus on the seasonal variability of the whole [Chl *a*] vertical distribution, confirm these previous statements. The climatological time-series of [Chl *a*] profiles (Fig. 3) for the South-Western region (Fig. 3b), the Ionian region (Fig. 3c) and the Levantine region (Fig. 3d) are very close to typical subtropical behavior marked by the quasi-permanent existence of the DCM (Letelier et al., 2004; Mignot et al., 2014). In particular, the [Chl *a*] climatology of the station BATS in the subtropical North Atlantic gyre (Steinberg et al., 2001; Lavigne et al., 2012) displays many similarities, in terms of ranges of values for [Chl *a*], DCM depths and depths of winter mixing, with the climatological time-series built in the Levantine Sea (Fig. 3d). The only main difference is that the "homogeneous" climatological profiles are observed from December in the Mediterranean regions and only from January at the BATS station (Lavigne et al., 2012). Regarding seasonal cycles obtained for the North-Western Mediterranean Sea, we can easily compared them to mid-latitude (40–60°) regions marked by an intense spring bloom like in the North Atlantic (Siegel et al., 2002) or in certain regions of the Southern Ocean (Thomalla et al., 2011). Similarly to our Mediterranean North-West observations, the seasonal cycles for [Chl *a*] vertical profiles presented by Boss et al. (2008) in the Western North-Atlantic (about 50° N) and by Chiswell (2011) in the waters east of New Zealand (about 40° S) display a majority of profiles with an "homogeneous" shape during winter and, at spring, a predominance





BGD
12, 4139–4181, 2015



of profiles displaying a "HSC" shape or an "homogeneous" shape with high [Chl *a*] values. The coexistence of "homogeneous" like and "HSC" like profiles during spring could be explained by the intermittent feature of mixing, which continuously modifies the vertical distribution of [Chl *a*] during spring bloom (Chiswell, 2011). Finally, it is important to mention that the summer situation is very different between the North-Atlantic region studied by Boss et al. (2008) and the North-Western Mediterranean Sea. Although, DCM like profiles are nearly permanent in the North-Western Mediterranean from May/June, Boss et al. (2008) observed them only from late summer.

Our analysis also showed that in the Mediterranean Sea, specific features of the "DCM" like [Chl *a*] profiles have a large variability. The most relevant indicator is certainly the DCM depth, which was observed to range between 30 m and more than 150 m. Its variability is partly explained by a seasonal and a spatial (longitudinal) component (Figs. 6 and 7). This seasonality of DCM is consistent with previous model results (Macias et al., 2014) and with individual Bio-Argo float observations (Mignot et al., 2014). The observed pattern in the seasonality of the DCM depth (i.e. deepening from spring to summer and shallowing from summer to autumn) was explained by Letelier et al. (2004) and Mignot et al. (2014). Authors supposed that the DCM depth is driven by the light availability and follows the depth of an isolume. The characterization of the deepening of the DCM with longitude (DCM deepens by 1.6 m per 1° of longitude east) obtained in the presented database is in agreement with previous review (Crise et al., 1999). However, it is not consistent with model results of Macias et al. (2014), which underestimate DCM depth in the Eastern Mediterranean Sea. Seasonal and longitudinal effects explain a part of the Mediterranean DCM variability but the "unexplained" part of DCM variability is significant. It could be ascribed to the interannual variability, especially in the North Ionian Sea which undergoes interannual reversals of its circulation (Civitarese et al., 2010) or to the numerous meso and submesoscale structures (i.e. gyres, fronts and jets) observed in the Mediterranean Sea (Hamad et al., 2005; Rio et al., 2007).





BGD
12, 4139–4181, 2015



Finally, the large variability of Mediterranean DCM like profiles allow us to analyze relationships between DCM characteristics and to compared them with the relationships determined from global ocean datasets (Mignot et al., 2011). The DCM characteristics analyzed here are the DCM depth, the width of the DCM (d$z$, see caption of Fig. 9 for details), the surface [Chl $a$] ([Chl $a$]$_{SURF}$) and the [Chl $a$] at DCM ([Chl $a$]$_{DCM}$). Scatter plots of [Chl $a$]$_{SURF}$ vs. DCM depth, [Chl $a$]$_{DCM}$ vs. DCM depth and d$z$ vs. [Chl $a$]$_{DCM}$ are displayed on Fig. 9a–c respectively. A second order polynomial model has been computed (blue lines on Fig. 9) on log transformed Mediterranean data and compared with the relationships obtained from a global ocean dataset (red lines on Fig. 9, Mignot et al., 2011). Although, for each case, similarities (at least in the sign of the slope) are observed, several differences, especially in the value of the slope, exists for the models [Chl $a$]$_{DCM}$ vs. DCM depth (Fig. 9b) and d$z$ vs. [Chl $a$]$_{DCM}$ (Fig. 9c). For a same DCM depth, [Chl $a$]$_{DCM}$ in the Mediterranean tends to be higher than in the global ocean and this trend is reinforced when DCM depth is shallow. This result may suggest that, in the Mediterranean Sea, production rate and biomass are particularly high at DCM when it ranges between 60 and 30 m. Regarding the relationship between d$z$ and [Chl $a$]$_{DCM}$, in the Mediterranean Sea, like in the global ocean, the width of the DCM is inversely related to its [Chl $a$]. However, this trend is reduced in the Mediterranean Sea compared to the global ocean. In the Mediterranean Sea, large DCMs have higher [Chl $a$]$_{DCM}$ than in global ocean and narrow DCMs have lower [Chl $a$]$_{DCM}$. It appears that for a same range of DCM widths the corresponding range of [Chl $a$]$_{DCM}$ is smaller in the Mediterranean Sea than in the global ocean.

## 5 Conclusion

Since the initial work of the MEDAR/MEDATLAS group (Maillard et al., 2005) renewed by Manca et al. (2004), the proposed study represents the first attempt to analyze the seasonal variations of the [Chl $a$] vertical distribution over the Mediterranean Sea. We updated here the picture of the [Chl $a$] field in the basin, which was mainly derived from





BGD
12, 4139–4181, 2015



surface satellite data or from limited and scarce in situ observations. Chlorophyll *a* fluorescence data (specifically calibrated and homogenized with a dedicated method) allowed for the production of a larger database than the commonly used in situ bottle estimations. Additionally, a better description of the vertical distribution was possible. 6790 profiles of fluorescence were gathered and processed to carry out a comprehensive analysis of the seasonal variability of the vertical [Chl *a*] profiles within the main Mediterranean sub-basins. The comparison of our [Chl *a*] database with the MEDATLAS climatology allowed to validate our fluorescence based [Chl *a*] data with in situ data derived from water samples but also to demonstrate that the characteristics of our new database highly contribute to improve our knowledge of [Chl *a*] vertical distribution in the Mediterranean Sea. Two complementary approaches have been used to analyze the database: the traditional construction of monthly mean [Chl *a*] profiles (Conkright et al., 2002) and an innovative approach which is based on the identification of the general shape of the fluorescence profile. The association of these two approaches allowed to stress the mean seasonal behavior as well as its variability and its stability. The use of this two complementary approaches was essential in the Mediterranean Sea where the shape of the [Chl *a*] is very dynamic, especially during winter. DCM appears as an important characteristic of [Chl *a*] vertical profile, as it is dominant in the Mediterranean Sea (53 % of available [Chl *a*] profiles). Our results also showed that different types of phytoplankton biomass annual dynamics co-exist in the Mediterranean Sea which confirms previous surface limited satellite findings (D'Ortenzio and Ribera d'Alcalà, 2009). Overall, from the phytoplankton dynamics point of view, Mediterranean Sea can be compared to some large regions of the global ocean.

The present study was often limited by the quantity of data which did not allow to analyze every regions of the Mediterranean Sea (e.g. the Adriatic Sea). We deplore the singular absence of fluorescence profiles in oceanographic databases compared to other parameters. For instance, in the MEDAR database, there are 118 009 profiles of salinity, 44 928 profiles of oxygen and only 1984 profiles of chlorophyll *a* fluorescence. Finally, in this study we were only able to present climatological behaviors. To





BGD
12, 4139–4181, 2015



better understand processes which impact on seasonal variability of the [Chl *a*] vertical profile, it would be necessary to study some particular cases showing, with a high frequency, annual series of vertical [Chl *a*] profiles. These data are now available with the development of Bio-Argo floats (Jonhson et al., 2009) and some studies have already demonstrated their potential for such applications (Boss and Behrenfeld, 2010; Mignot et al., 2014).

*Acknowledgements.* The authors would like to thank all people involved in the collection and distribution of oceanographic data used in this paper. We thank PANGAEA, SISMER, the National Oceanographic Data Center and the OGS data center for making data freely available online. The programs LEFE-CYBER, Bio-Argo, MEDAR and IP SESAME are thanks for their valuable contribution to Mediterranean databases. The U.S. NASA Agency is thanked for the easy access to SeaWiFS and MODIS data. We acknowledge the support of the European Commission "Cofunded by the European Union under FP7-People – Co-funding of Regional, National and International Programmes, GA n. 600407" and of the RITMARE Flagship Project. This work is also the contribution to the PABO (Plateformes Autonomes and Biogeochimie Oceanique) funded by the ANR, to the French "Equipement d'Avenir" NAOS project (ANR J11R107-F) and to the remOcean project funded by the grant agreement No. 246777. We are also grateful to Louis Prieur and Julia Uitz for constructive comments and suggestions.

## References

Andersen, V. and Prieur, L.: One-month study in the open nw mediterranean sea (dynaproc experiment, may 1995): overview of the hydrobiogeochemical structures and effects of wind events, Deep-Sea Res. Pt. I, 47, 397–422, 2000.

Antoine, D., Morel, A., and André, J.-M.: Algal pigment distribution and primary production in the eastern Mediterranean as derived from coastal zone color scanner observations, J. Geophys. Res., 100, 16193–16209, doi:10.1029/95JC00466, 1995.

Barale, V., Jaquet, J.-M., and Ndiaye, M.: Algal blooming patterns and anomalies in the Mediterranean Sea as derived from the SeaWiFS data set (1998–2003), Remote Sens. Environ., 112, 3300–3313, doi:10.1016/j.rse.2007.10.014, 2008.





BGD
12, 4139–4181, 2015



Bosc, E., Bricaud, A., and Antoine, D.: Seasonal and interannual variability in algal biomass and primary production in the Mediterranean Sea, as derived from 4 years of SeaWiFS observations, Global Biogeochem. Cy., 18, GB1005, doi:10.1029/2003GB002034, 2004.

Boss, E. and Behrenfeld, M.: In situ evaluation of the initiation of the North Atlantic phytoplankton bloom, Geophys. Res. Lett., 37, L18603, doi:10.1029/2010GL044174, 2010.

Boss, E., Swift, D., Taylor, L., Brickley, P., Zaneveld, R., Riser, S., Perry, M., and Strutton, P.: Observations of pigment and particle distributions in the western North Atlantic from an autonomous float and ocean color satellite, Limnol. Oceanogr., 53, 2112–2122, doi:10.4319/lo.2008.53.5_part_2.2112, 2008.

Boyer, T. P., Antonov, J. I., Baranova, O. K., Carla, C., Garcia, H. E., Grodsky, A., Johnson, D. R., Locarnini, R. A., Mishonov, A. V., O'Brien, T. D., Paver, C. R., Reagan, J. R., Seidov, D., Smolyar, I. V., and Zwengan, M. M.: World Ocean Database 2013, edited by: Levitus, S. and Mishonov, A., NOAA Atlas NESDIS, 72, 209 pp., 1315 East-West Highway, Silver Spring, 2013.

Cetinic, I., Toro-Farmer, G., Ragan, M., Oberg, C., and Jones, B.: Calibration procedure for Slocum glider deployed optical instruments, Opt. Express, 17, 15420–15430, 2009.

Chiswell, S.: Annual cycles and spring blooms in phytoplankton: don't abandon Sverdrup completely, Mar. Ecol.-Prog. Ser., 443, 39–50, 2011.

Christaki, U., Giannakourou, A., Van Wambeke, F., and Grégori, G.: Nanoflagellate predation on auto-and heterotrophic picoplankton in the oligotrophic Mediterranean Sea, J. Plankton Res., 23, 1297–1310, 2001.

Civitarese, G., Gačić, M., Lipizer, M., and Eusebi Borzelli, G. L.: On the impact of the Bimodal Oscillating System (BiOS) on the biogeochemistry and biology of the Adriatic and Ionian Seas (Eastern Mediterranean), Biogeosciences, 7, 3987–3997, doi:10.5194/bg-7-3987-2010, 2010.

Claustre, H., Fell, F., Oubelkheir, K., Prieur, L., Sciandra, A., Gentili, B., and Babin, M.: Continuous monitoring of surface optical properties across a geostrophic front: biogeochemical inferences, Limnol. Oceanogr., 45, 309–321, 2000.

Claustre, H., Hooker, S. B., Van Heukelem, L., Berthon, J- F., Barlow, R., Ras, J., Sessions, S., Targa, C., Thomas, C. S., van der Linde, D., and Marty, J. C.: An intercomparison of hplc phytoplankton pigment methods using in situ samples: application to remote sensing and database activities, Mar. Chem., 85, 41–61, 2004.





BGD
12, 4139–4181, 2015



Conkright, M., O'Brien, T., Stephens, K., Locarnini, R., Garcia, H., Boyer, T., and Antonov, J.: World Ocean Atlas 2001, Vol. 6, Chlorophyll, edited by: Levitus, S., NOAA Atlas NESDIS, 54, US Governement Printing Office, Washington, DC, 46 pp., 2002.

Crise, A., Allen, J., Baretta, J., Crispi, G., Mosetti, R., and Solidoro, C.: The Mediterranean pelagic ecosystem response to physical forcing, Prog. Oceanogr., 44, 219–243, doi:10.1016/S0079-6611(99)00027-0, 1999.

Cullen, J.: The deep chlorophyll maximum – comparing vertical profiles of Chlorophyll-A, Can. J. Fish. Aquat. Sci., 39, 791–803, 1982.

Cullen, J. and Lewis, M.: Biological processes and optical measurements near the sea surface: some issues relevant to remote sensing, J. Geophys. Res.-Oceans, 100, 13255–13266, 1995.

de Boyer Montegut, C., Madec, G., Fischer, A., Lazar, A., and Iudicone, D.: Mixed layer depth over the global ocean: an examination of profile data and a profile-based climatology, J. Geophys. Res., 109, C12003, doi:10.1029/2004JC002378, 2004.

Devred, E., Sathyendranath, S., and Platt, T.: Delineation of ecological provinces using ocean colour radiometry, Mar. Ecol.-Prog. Ser., 346, 1–13, 2007.

Dolan, J., Vidussi, F., and Claustre, H.: Planktonic ciliates in the Mediterranean Sea: longitudinal trends, Deep-Sea Res. Pt. I, 46, 2025–2039, doi:10.1016/S0967-0637(99)00043-6, 1999.

Dolan, J., Claustre, H., Carlotti, F., Plounevez, S., and Moutin, T.: Microzooplankton diversity: relationships of tintinnid ciliates with resources, competitors and predators from the Atlantic Coast of Morocco to the Eastern Mediterranean, Deep-Sea Res. Pt. I, 49, 1217–1232, doi:10.1016/S0967-0637(02)00021-3, 2002.

D'Ortenzio, F. and Ribera d'Alcalà, M.: On the trophic regimes of the Mediterranean Sea: a satellite analysis, Biogeosciences, 6, 139–148, doi:10.5194/bg-6-139-2009, 2009.

D'Ortenzio, F., Iudicone, D., Montegut, C., Testor, P., Antoine, D., Marullo, S., Santoleri, R., and Madec, G.: Seasonal variability of the mixed layer depth in the Mediterranean Sea as derived from in situ profiles, Geophys. Res. Lett., 32, L12605, doi:10.1029/2005GL022463, 2005.

D'Ortenzio, F., Thierry, V., Eldin, G., Claustre, H., Testor, P., Coatanoan, C., Tedetti, M., Guinet, C., Poteau, A., Prieur, L., Lefevre, D., Bourrin, F., Carval, T., Goutx, M., Garçon, V., Thouron, D., Lacombe, M., Lherminier, P., Loisel, H., Mortier, L., and Antoine, D.: White Book on Oceanic Autonomous Platforms for Biogeochemical Studies: Instrumentation and Measure (PABIM) version 1.3, Villefranche sur mer, available at: http://www.coriolis.eu.org/News-Events/Latest-News/PABIM-White-BOOK, last access: 25 February 2015, 2010.





BGD
12, 4139–4181, 2015



D'Ortenzio, F., Lavigne, H., Besson, F., Claustre, H., Coppola, L., Garcia, N., Laes-Huon, A., Le Reste, S., Malardé, D., Migon, C., Morin, P., Mortier, L., Poteau, A., Prieur, L., Raimbault, P., and Testor, P.: Observing mixed layer depth, nitrate and chlorophyll concentrations in the northwestern Mediterranean: a combined satellite and $NO_3$ profiling floats experiment, Geophys. Res. Lett., 41, 6443–6451, doi:10.1002/2014GL061020, 2014.

Dugdale, R. and Wilkerson, F.: Nutrient sources and primary production in the Eastern Mediterranean, Oceanol. Acta, 9, 179–184, 1988.

Durrieu de Madron, X., Guieu, C., Sempéré, R., et al.: Marine ecosystems responses to climatic and anthropogenic forcings in the mediterranean, Prog. Oceanogr., 91, 97–166, 2011.

Estrada, M., Marrase, C., Latasa, M., Berdalet, E., Delgado, M., and Riera, T.: Variability of deep chlorophyll maximum characteristics in the Northwestern Mediterranean, Mar. Ecol.-Prog. Ser., 92, 289–289, 1993.

Feldman, G., Kuring, N., Ng, C., Esaias, W., McClain, C., Elrod, J., Maynard, N., and Endres, D.: Ocean-color: availability of the global data set, EOS T. Am. Geophys. Un., 70, 634–641, 1989.

Franz, B., Werdell, P., Meister, G., Bailey, S., Eplee, R., Feldman, G., Kwiatkowskaa, E., McClain, C., Patt., F., and Thomas, D.: The continuity of ocean color measurements from SeaWiFS to MODIS, in: Earth Observing Systems: X. Proceedings SPIE, vol. 5882, edited by: Butler, J. J., The International Society for Optical Engineering, 1–13, 2005.

Gieskes, W. W. and Kraay, G. W.: Unknown chlorophyll *a* derivatives in the North Sea and the Tropical Atlantic Ocean revealed by HPLC Analysis, Limnol. Oceanogr., 28, 757–766, 1983.

Hamad, N., Millot, C., and Taupier-Letage, I.: A new hypothesis about the surface circulation in the eastern basin of the mediterranean sea, Prog. Oceanogr., 66, 287–298, doi:10.1016/j.pocean.2005.04.002, 2005.

Ignatiades, L., Gotsis-Skretas, O., Pagou, K., and Krasakopoulou, E.: Diversification of phytoplankton community structure and related parameters along a large-scale longitudinal east–west transect of the Mediterranean Sea, J. Plankton Res., 31, 411–428, 2009.

Johnson, K. S., Berelson, W. M., Boss, E. S., Chase, Z., Claustre, H., Emerson, S. R., Gruber, N., Kortzinger, A., Perry, M. J., and Riser, S. C.: Observing biogeochemical cycles at global scales with profiling floats and gliders: prospects for a global array, Oceanography, 22, 216–225, 2009.

Kiefer, D. A.: Fluorescence properties of natural phytoplankton populations, Mar. Biol., 22, 263–269, 1973.





BGD
12, 4139–4181, 2015



Kolber, Z. and Falkowski, P. G.: Use of active fluorescence to estimate phytoplankton photosynthesis in situ, Limnol. Oceanogr., 38, 1646–1665, 1993.
Krom, M., Brenner, S., Kress, N., Neori, A., and Gorgon, L.: Nutrient dynamics and new production in a warm-core Eddy from the Eastern Mediterranean-Sea, Deep-Sea Res. Pt. I, 39, 467–480, 1992.
Lavigne, H., D'Ortenzio, F., Claustre, H., and Poteau, A.: Towards a merged satellite and in situ fluorescence ocean chlorophyll product, Biogeosciences, 9, 2111–2125, doi:10.5194/bg-9-2111-2012, 2012.
Lavigne, H., D'Ortenzio, F., Migon, C., Claustre, H., Testor, P., d'Alcalà, M. R., Lavezza, R., Houpert, L., and Prieur, L.: Enhancing the comprehension of mixed layer depth control on the Mediterranean phytoplankton phenology, J. Geophys. Res.-Oceans, 118, 3416–3430, doi:10.1002/jgrc.20251, 2013.
Letelier, R. M., Karl, D. M., Abbott, M. R., and Bidigare, R. R.: Light driven seasonal patterns of chlorophyll and nitrate in the lower euphotic zone of the North Pacific subtropical gyre, Limnol. Oceanogr., 49, 508–519, 2004.
Longhurst, A. R.: Ecological Geography of the Sea, 2nd Edn., Academic Press, San Diego, 2006.
Longhurst, A. R. and Harrison, G. W.: The biological pump: profiles of plankton production and consumption in the upper ocean, Prog. Oceanogr., 22, 47–123, 1989.
Lorenzen, C. J.: A method for the continuous measurement of in vivo chlorophyll concentration, Deep-Sea Res., 13, 223–227, 1966.
Macias, D., Stips, A., and Garcia-Gorriz, E.: The relevance of deep chlorophyll maximum in the open Mediterranean Sea evaluated through 3D hydrodynamic-biogeochemical coupled simulations, Ecol. Model., 281, 26–37, 2014.
Maillard, C. and Coauthors, 2005: MEDAR/MEDATLAS 1998–2001: A Mediterranean and Black Sea oceanographic data base and network, Boll. Geofis. Teor. Appl., 46, 329–344, 2005.
Manca, B., Burca, M., Giorgetti, A., Coatanoan, C., Garcia, M.-J., and Iona, A.: Physical and biochemical averaged vertical profiles in the Mediterranean regions: an important tool to trace the climatology of water masses and to validate incoming data from operational oceanography, J. Marine Syst., 48, 83–116, 2004.
Marty, J.-C., Chiaverini, J., Pizay, M.-D., and Avril, B.: Seasonal and interannual dynamics of nutrients and phytoplankton pigments in the western Mediterranean Sea at the DYFAMED





BGD
12, 4139–4181, 2015



time-series station (1991–1999), Deep-Sea Res. Pt. II, 49, 1965–1985, doi:10.1016/S0967-0645(02)00022-X, 2002.
McClain, C., Cleave, M., Feldman, G., Gregg, W., Hooker, S., and Kuring, N.: Science quality SeaWiFS data for global biosphere research, Sea Technol., 39, 10–16, 1998.
Mignot, A., Claustre, H., D'Ortenzio, F., Xing, X., Poteau, A., and Ras, J.: From the shape of the vertical profile of in vivo fluorescence to Chlorophyll-*a* concentration, Biogeosciences, 8, 2391–2406, doi:10.5194/bg-8-2391-2011, 2011.
Mignot, A., Claustre, H., Uitz, J., Poteau, A., D'Ortenzio, F., and Xing, X.: Understanding the seasonal dynamics of phytoplankton biomass and the deep chlorophyll maximum in oligotrophic environments: a Bio-Argo float investigation, Global Biogeochem. Cy., 28, 856–876, 2014.
Muller, P., Li, X.-P., and Niyogi, K. K.: Non-photochemical quenching. A response to excess light energy, Plant Physiol., 125, 1558–1566, doi:10.1104/pp.125.4.1558, 2001.
Morel, A. and André, J.-M.: Pigment distribution and primary production in the western Mediterranean as derived and modeled from coastal zone color scanner observations, J. Geophys. Res., 96, 12685–12698, doi:10.1029/91JC00788, 1991.
Morel, A. and Berthon, J.: Surface pigments, algal biomass profiles, and potential production of the euphotic layer – relationships reinvestigated in view of remote-sensing applications, Limnol. Oceanogr., 34, 1545–1562, 1989.
Morel, A. and Maritorena, S.: Bio-optical properties of oceanic waters: a reappraisal, J. Geophys. Res.-Oceans, 106, 7163–7180, 2001.
Moutin, T. and Prieur, L.: Influence of anticyclonic eddies on the Biogeochemistry from the Oligotrophic to the Ultraoligotrophic Mediterranean (BOUM cruise), Biogeosciences, 9, 3827–3855, doi:10.5194/bg-9-3827-2012, 2012.
Moutin, T. and Raimbault, P.: Primary production, carbon export and nutrients availability in western and eastern Mediterranean Sea in early summer 1996 (MINOS cruise), J. Marine Syst., 33–34, 273–288, doi:10.1016/S0924-7963(02)00062-3, 2002.
Moutin, T., Van Wambeke, F., and Prieur, L.: Introduction to the Biogeochemistry from the Oligotrophic to the Ultraoligotrophic Mediterranean (BOUM) experiment, Biogeosciences, 9, 3817–3825, doi:10.5194/bg-9-3817-2012, 2012.
Navarro, G., Vázquez, Á., Macás, D., Bruno, M., and Ruiz, J.: Understanding the patterns of biological response to physical forcing in the Alborán Sea (western Mediterranean), Geophys. Res. Lett., 38, L23606, doi:10.1029/2011GL049708, 2011.





BGD
12, 4139–4181, 2015



Platt, T., Sathyendranath, S., White III, G. N., Fuentes-Yaco, C., Zhai, L., Devred, E., and Tang, C.: Diagnostic properties of phytoplankton time series from remote sensing, Estuar. Coast., 33, 428–439, 2010.

Psarra, S., Tselepides, A., and Ignatiades, L.: Primary productivity in the oligotrophic Cretan Sea (NE Mediterranean): seasonal and interannual variability, Prog. Oceanogr., 46, 187–204, 2000.

Rio, M.-H., Poulain, P.-M., Pascual, A., Mauri, E., Larnicol, G., and Santoleri, R.: A mean dynamic topography of the Mediterranean Sea computed from altimetric data, in-situ measurements and a general circulation model, J. Marine Syst., 65, 484–508, 2007.

Sharples, J., Moore, C. M., Rippeth, T. P., Holligan, P. M., Hydes, D. J., Fisher, N. R., and Simpson, J. H.: Phytoplankton distribution and survival in the thermocline, Limnol. Oceanogr., 46, 486–496, 2001.

Siegel, D. A., Doney, S. C., and Yoder, J. A.: The North Atlantic spring phytoplankton bloom and sverdrup's critical depth hypothesis, Science, 296, 730–733, doi:10.1126/science.1069174, 2002.

Siokou-Frangou, I., Christaki, U., Mazzocchi, M. G., Montresor, M., Ribera d'Alcalá, M., Vaqué, D., and Zingone, A.: Plankton in the open Mediterranean Sea: a review, Biogeosciences, 7, 1543–1586, doi:10.5194/bg-7-1543-2010, 2010.

Sosik, H. M., Chisholm, S. C., and Olson, R. J.: Chlorophyll fluorescence from single cells: interpretation of flow cytometric signals, Limnol. Oceanogr., 34, 1749–1761, 1989.

Steinberg, D., Carlson, C., Bates, N., Johnson, R., Michaels, A., and Knap, A.: Overview of the US JGOFS Bermuda Atlantic time-series study (BATS): a decade-scale look at ocean biology and biogeochemistry, Deep-Sea Res. Pt. II, 48, 1405–1447, 2001.

Strass, V.: On the calibration of large-scale fluorometric chlorophyll measurements from towed undulating vehicles, Deep-Sea Res. Pt. I., 37, 525–540, doi:10.1016/0198-0149(90)90023-O, 1990.

Strickland, J.: Production of organic matter in primary stages of the marine food chain, in: Chemical Oceanography, edited by: Riley, J. P. and Skirrow, G., Academic Press, London, 477–610, 1965.

Taupier-Letage, I., Puillat, I., Millot, C., and Raimbault, P.: Biological response to mesoscale eddies in the Algerian Basin, J. Geophys. Res., 108, 3245, doi:10.1029/1999JC000117, 2003.





BGD
12, 4139–4181, 2015



Thomalla, S. J., Fauchereau, N., Swart, S., and Monteiro, P. M. S.: Regional scale characteristics of the seasonal cycle of chlorophyll in the Southern Ocean, Biogeosciences, 8, 2849–2866, doi:10.5194/bg-8-2849-2011, 2011.

Uitz, J., Claustre, H., Morel, A., and Hooker, S.: Vertical distribution of phytoplankton communities in open ocean: an assessment based on surface chlorophyll, J. Geophys. Res., 111, C08005, doi:10.1029/2005JC003207, 2006.

Volpe, G., Nardelli, B. B., Cipollini, P., Santoleri, R., and Robinson, I. S.: Seasonal to interannual phytoplankton response to physical processes in the Mediterranean Sea from satellite observations, Remote Sens. Environ., 117, 223–235, doi:10.1016/j.rse.2011.09.020, 2012.

Ward, B. A. and Waniek, J. J.: Phytoplankton growth conditions during autumn and winter in the Irminger Sea, North Atlantic, Mar. Ecol.-Prog. Ser., 334, 47–61, 2007.

Winn, C. D., Campbell, L., Christian, J. R., Letelier, R. M., Hebel, D. V., Dore, J. E., Fujieki, L., and Karl, D. M.: Seasonal variability in the phytoplankton community of the North Pacific Subtropical Gyre, Global Biogeochem. Cy., 9, 605–620, doi:10.1029/95GB02149, 1995.

Xing, X., Morel, A., Claustre, H., Antoine, D., D'Ortenzio, F., Poteau, A., and Mignot, A.: Combined processing and mutual interpretation of radiometry and fluorimetry from autonomous profiling Bio-Argo floats: chlorophyll *a* retrieval, J. Geophys. Res., 116, C06020, doi:10.1029/2010JC006899, 2011.

Xing, X., Claustre, H., Blain, S., D'Ortenzio, F., Antoine, D., Ras, J., and Guinet, C.: Quenching correction for in vivo chlorophyll fluorescence measured by instrumented elephant seals in the Kerguelen region (Southern Ocean), Limnol. Oceanogr.-Meth., 10, 483–495, 2012.

Yoder, J. A., McClain, C. R., Feldman, G. C., and Esaias, W. E.: Annual cycles of phytoplankton chlorophyll concentrations in the global ocean: a satellite view, Global Biogeochem. Cy., 7, 181–193, doi:10.1029/93GB02358, 1993.





BGD
12, 4139–4181, 2015



**Table 1.** Description of sources for fluorescence profiles. In this table, only fluorescence profiles achieved in Mediterranean regions where bathymetry is superior to 100 m are counted. Coastal regions have been neglected.

| | Data source | Number of profiles |
|---|---|---|
| Online databases | PANGAEA (http://www.pangaea.de/) | 93 |
| | SISMER (http://www.ifremer.fr/sismer/index_FR.htm) | 110 |
| | WOD09 (http://www.nodc.noaa.gov/) | 94 |
| | OGS database (http://nodc.ogs.trieste.it/cocoon/data/parameters) | 689 |
| SUB-TOTAL | | 986 |
| French cruises | PROSOPE (Claustre et al., 2004) | 96 |
| | DYNAPROC (Andersen and Prieur, 2000) | 251 |
| | BOUM (Moutin et al., 2012) | 573 |
| | ALMOFRONT (Claustre at al., 2000) | 1046 |
| | DYFAMED (Marty et al., 2002) | 191 |
| | MOOSE-GE (http://hermes.dt.insu.cnrs.fr/moose/) | 285 |
| | DEWEX (Durrieu de Madron et al., 2011) | 228 |
| SUB-TOTAL | | 2670 |
| SESAME Program (http://www.sesame-ip.eu/) | | 1815 |
| MEDAR Program (MEDAR Group., 2002) | | 228 |
| Bio-Argo (Xing et al., 2011; http://www.oao.obs-vlfr.fr/web/index.php) | | 1091 |
| TOTAL | | 6790 |





BGD
12, 4139–4181, 2015



**Table 2.** Averaged [Chl *a*] at DCM for each geographical point analyzed on Fig. 3 (i.e. yellow diamonds on Fig. 1). Averaged [Chl *a*] values were computed by averaging all the DCM depth [Chl *a*] estimations extracted from available "DCM" like profiles.

| | Point: 42° N 5° E (North-West) | | | Point: 38° N 5° E (South-West) | | | Point: 36° N 17° E (Ionian) | | | Point: 33.5° N 33° E (Levantine) | | |
|---|---|---|---|---|---|---|---|---|---|---|---|---|
| | MEAN | SD | *N* | MEAN | SD | *N* | MEAN | SD | *N* | MEAN | SD | *N* |
| Apr | 1.22 | 0.66 | 26 | | | | 0.73 | 0.24 | 107 | 0.50 | 0.07 | 6 |
| May | 0.86 | 0.20 | 38 | 0.93 | 0.18 | 9 | 0.73 | 0.24 | 37 | 0.50 | 0.09 | 6 |
| Jun | 0.99 | 0.28 | 129 | 1.24 | 0.76 | 6 | 0.90 | 0.23 | 17 | 0.47 | 0.09 | 154 |
| Jul | 0.98 | 0.40 | 67 | 0.86 | 0.17 | 160 | 0.47 | 0.15 | 9 | 0.46 | 0.15 | 10 |
| Aug | 0.69 | 0.32 | 45 | 0.84 | 0.40 | 7 | 0.44 | 0.14 | 22 | 0.44 | 0.12 | 11 |
| Sep | 0.65 | 0.26 | 41 | 0.99 | 0.98 | 9 | 0.34 | 0.11 | 23 | 0.34 | 0.07 | 23 |
| Oct | 0.90 | 0.45 | 33 | 1.06 | 0.10 | 6 | 0.48 | 0.24 | 81 | 0.31 | 0.04 | 10 |





BGD
12, 4139–4181, 2015



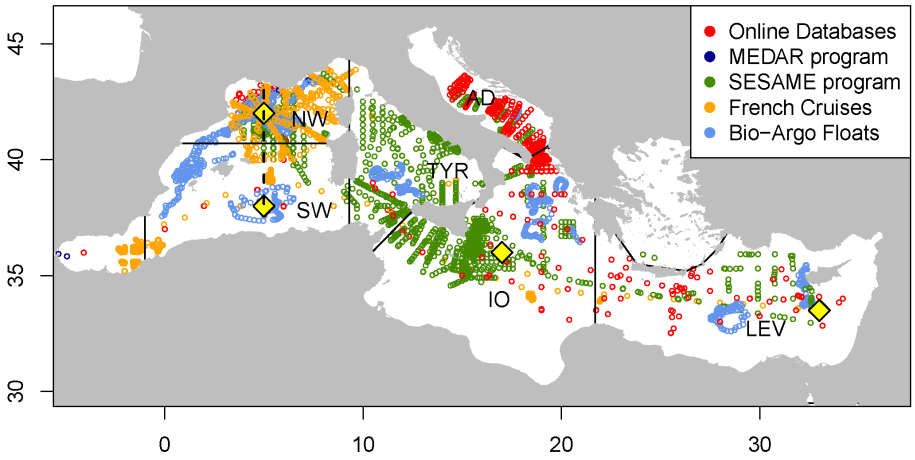


**Figure 1.** Spatial distribution of fluorescence profiles available in the database. Colors indicate the source of data. Black lines delineate large Mediterranean regions: they are referred by NW for "North-West", SW for "South-West", TYR for "Tyrrhenian", AD for "Adriatic", IO for "Ionian" and LEV for "Levantine". Yellow diamonds refer to the center of region for which a climatology of [Chl *a*] vertical profile has been computed (see Fig. 3) and the dashed black line shows the center of the North-West transect (see Fig. 4).





BGD
12, 4139–4181, 2015



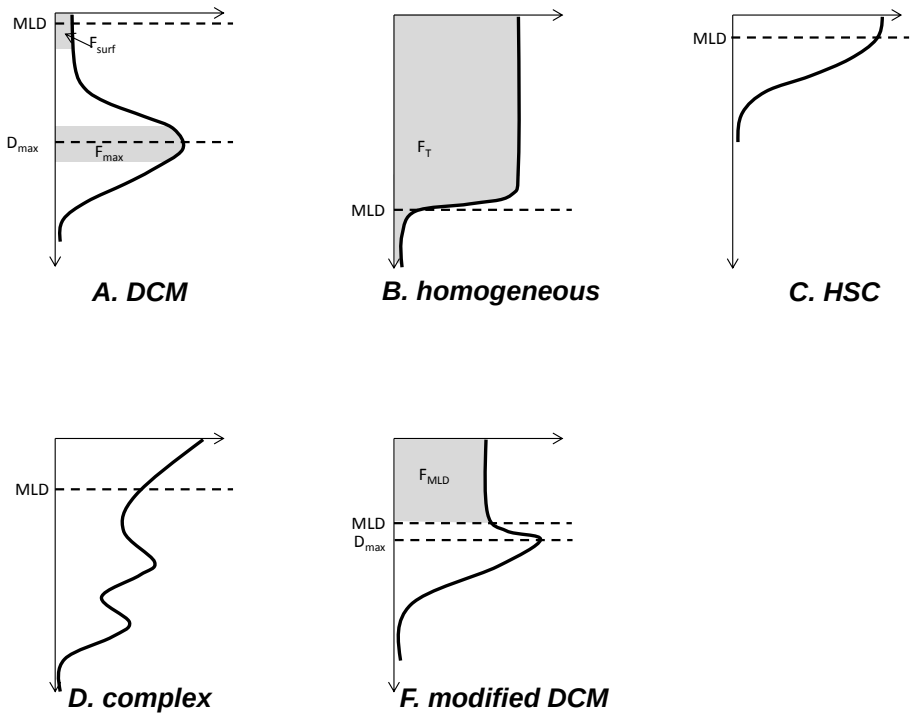


**Figure 2.** The five standard shapes for [Chl *a*] vertical profiles identified in our dataset. See Sect. 2.3 of the text for more details about these shapes and for a description of the algorithm used to identify them. Black solid lines represent the normalized [Chl *a*] vertical profile. Metrics used for the determination of the profile standard shape (i.e. MLD, $D_{max}$, $F_{surf}$, $F_{max}$, $F_T$, see text Sect. 2.3 for definitions) are represented on standard profiles. Although all of these metrics have been computed on each fluorescence profile, they could not be represented on a same profile for practical reasons.





BGD
12, 4139–4181, 2015



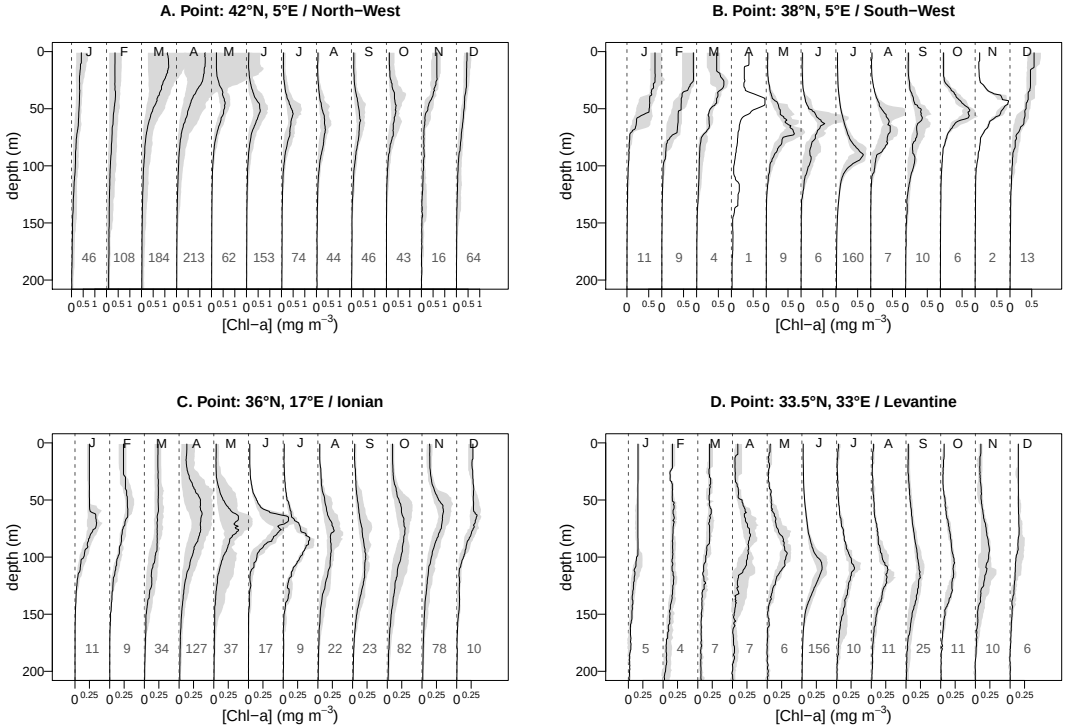


**Figure 3.** Climatology of [Chl *a*] vertical profiles for 4 points of the Mediterranean Sea (see yellow diamonds on Fig. 1). All profiles located within a 4° × 4° box centered on indicated positions were retained. The median value for each month is the black line. The grey zone indicates the 0.1–0.9 quantile range. Numbers below climatological profiles indicate on the number of available data profiles used to compute them.





BGD
12, 4139–4181, 2015



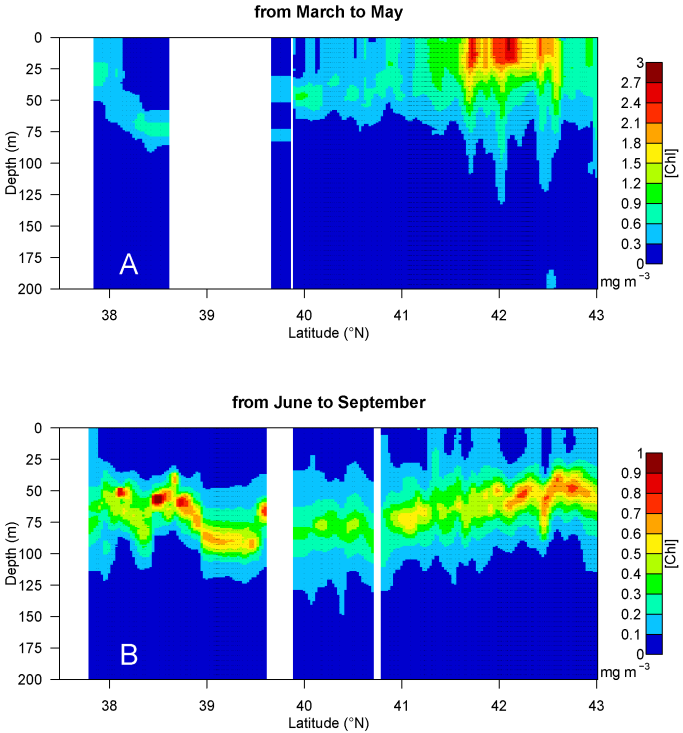


**Figure 4.** North–South climatological transect of [Chl *a*] along the 5° W meridian (see the black dotted line on Fig. 1). **(a)** represents the averaged situation for the March–May period and **(b)** for the June–September period. Note that color scales are different between (**a** and **b**). For each available data profile, a vertical dotted line was superimposed to the graphic.





BGD
12, 4139–4181, 2015



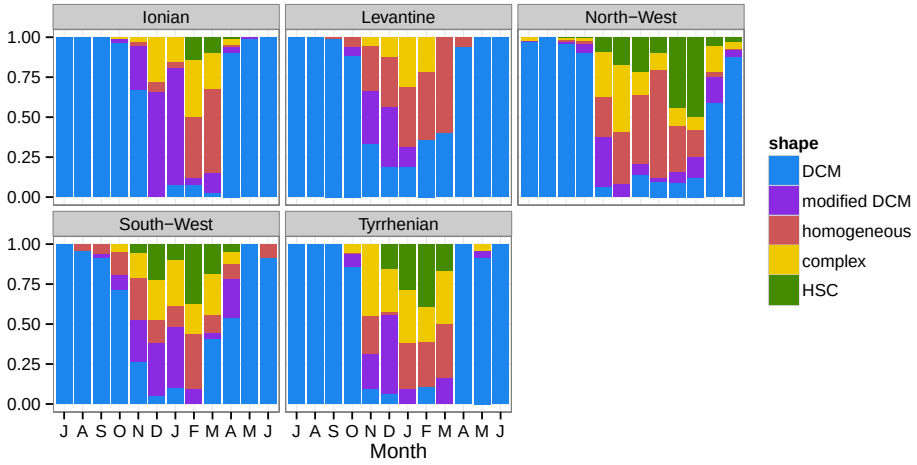


**Figure 5.** Histograms indicating for each month and each Mediterranean region, the proportion of each type of standard shape observed in the 1994–2014 database (i.e. “DCM”, “homogeneous”, “HSC”, “modified DCM” and “complex” see Fig. 2 and Sect. 2.3). The height of color bars indicates on the proportion of profiles which were classed in each category of standard shapes. Note that months are ranging from July to June.





BGD
12, 4139–4181, 2015



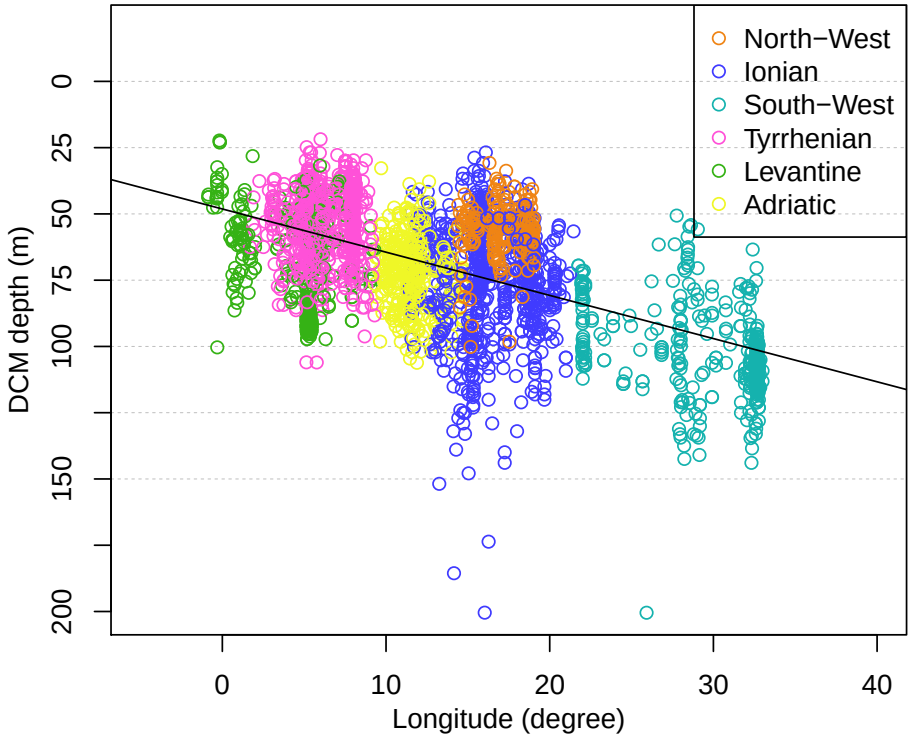


**Figure 6.** DCM depth as a function of longitude. DCM depths were computed only on "DCM" like profiles (see Sect. 2.3 for an objective definition of "DCM" like profile). Black line represents the linear model between the DCM depth and the longitude. Its slope is 1.6 m per degree of longitude.





BGD
12, 4139–4181, 2015



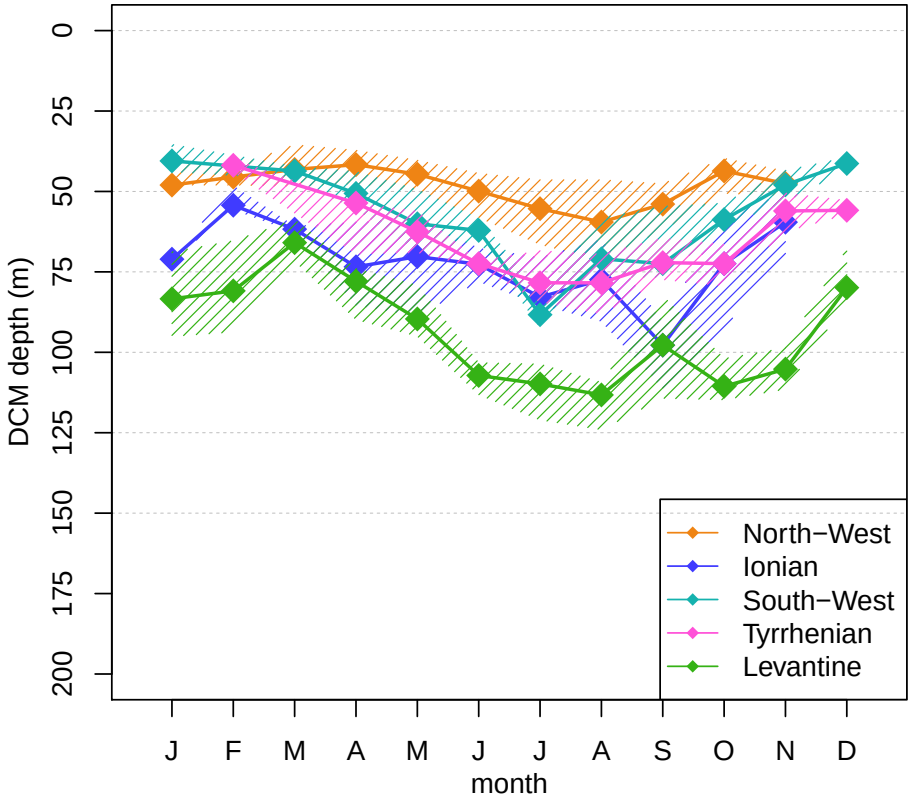


**Figure 7.** Seasonal evolution of the DCM depth. DCM depths were computed only on "DCM" like profiles (see Sect. 2.3 for an objective definition of "DCM" like profile). Diamonds refer to monthly median whereas hatched zones indicate the inter-quartile range.





BGD
12, 4139–4181, 2015



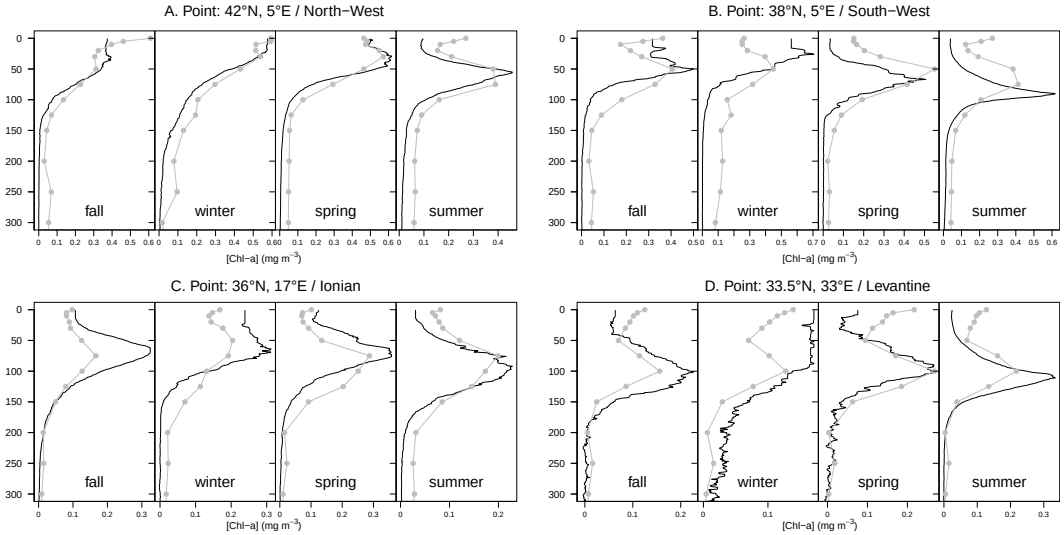


**Figure 8.** [Chl *a*] profiles obtained from the MEDATLAS climatology for the four locations analyzed on Fig. 3 (grey lines and grey points). MEDATLAS climatology was download on http://modb.oce.ulg.ac.be/backup/medar/medar_med.html. For comparison, corresponding seasonally averaged profiles were computed from the 1998–2014 [Chl *a*] fluorescence database (black lines).





BGD
12, 4139–4181, 2015



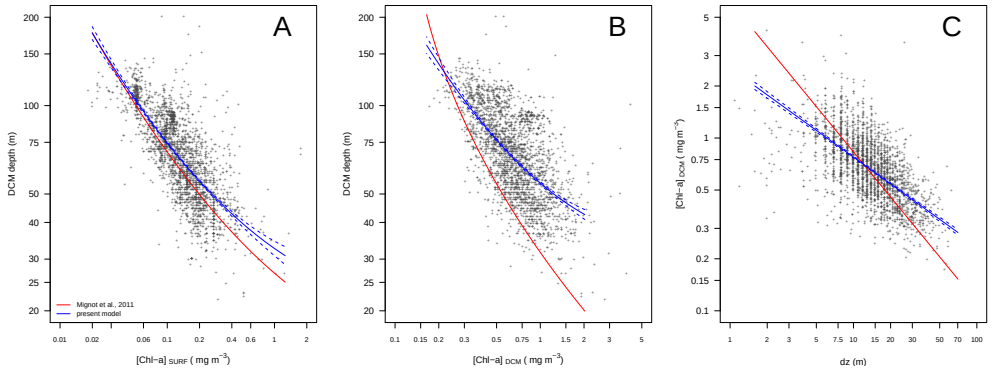


**Figure 9.** Scatter plots of the DCM depth as a function of surface [Chl *a*] **(a)**, of the DCM depth as a function of [Chl *a*] at DCM **(b)** and of the width of the DCM (d*z*) as a function of the [Chl *a*] at DCM **(c)**. Only "DCM" like profiles were used for this analysis. Similarly to Mignot et al. (2011), d*z* was determined by applying a Gaussian model on the [Chl *a*] profiles. Surface [Chl *a*] comes from satellite ocean color data and the [Chl *a*] at DCM was extracted from satellite calibrated profiles. On each panel, the blue solid line refers to a second order polynomial model determined from present data with its confidence intervals (blue dotted lines). The red lines represent the models computed by Mignot et al. (2011) from a global ocean dataset.





BGD
12, 4139–4181, 2015